# *Mixed oxide semiconductors based on bismuth for photoelectrochemical applications*

**J. L. Ropero-Vega, A. M. Meléndez, J. A. Pedraza-Avella, Roberto J. Candal & M. E. Niño-Gómez**

**Journal of Solid State Electrochemistry**
Current Research and Development in Science and Technology

ISSN 1432-8488
Volume 18
Number 7

J Solid State Electrochem (2014)
18:1963-1971
DOI 10.1007/s10008-014-2420-4

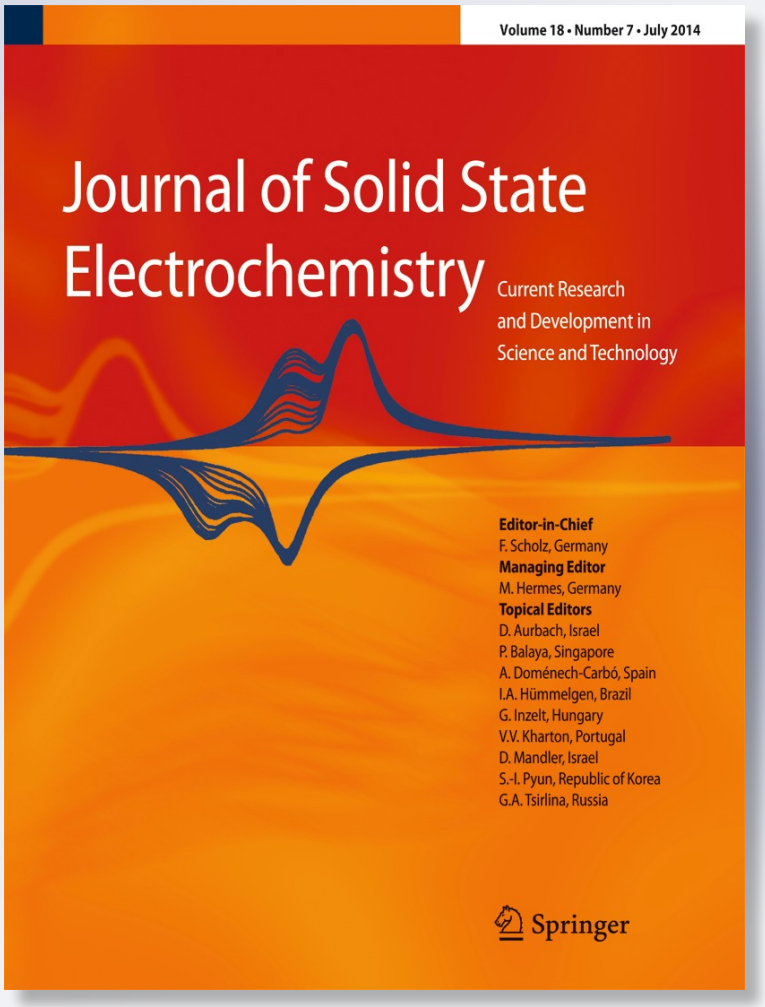


Springer

J Solid State Electrochem (2014) 18:1963–1971
DOI 10.1007/s10008-014-2420-4

ORIGINAL PAPER

# Mixed oxide semiconductors based on bismuth for photoelectrochemical applications

**J. L. Ropero-Vega · A. M. Meléndez · J. A. Pedraza-Avella · Roberto J. Candal · M. E. Niño-Gómez**

Received: 24 September 2013 / Revised: 1 December 2013 / Accepted: 18 December 2013 / Published online: 12 March 2014


**Abstract** The structural and photoelectrochemical properties of mixed oxide semiconductor films of Bi-Nb-M-O (M = Al, Fe, Ga, In) were studied in order to explore their use as photoanodes in photoelectrochemical cells. These films were prepared on AISI/SAE 304 stainless steel plates by sol–gel dip-coating. The films were characterized by scanning electron microscopy—energy dispersive spectroscopy (SEM-EDS), X-ray diffraction (XRD), and X-ray photoelectron spectroscopy (XPS), and their photoelectrochemical properties were studied by open circuit potential (OCP) measurements, linear sweep voltammetry (LSV), and cyclic voltammetry (CV). SEM micrographs show homogeneous and rough films with agglomerates on the surface. EDS analyses show that the films are composed of Bi, Nb, and M, and the agglomerates are mainly composed of Bi. XRD analyses show a predominant crystalline phase of bismuth(III) oxide ($Bi_2O_3$) and a secondary phase composed of Bi-M mixed oxides. It is noteworthy that there was no identified niobium-based crystalline phase. XPS results reveal that the films are composed by Bi(III), Nb(V), and M(III). CV results show that the electrochemical behavior is attributed only to the semiconductor films which indicate a good coating of the stainless steel support. OCP measurements show that all the films have n-type semiconductor properties and exhibited photoresponse to the visible light irradiation. LSV results show that the application of a potential higher than +0.1 V enhances the photocurrent which can be attributed to an improved charge carrier separation. The results indicate that these materials can be used in photoelectrochemical cells.

**Keywords** Sol–gel · Dip-coating · Bismuth oxide · Photoelectrochemistry · Visible light radiation

**Electronic supplementary material** The online version of this article (doi:10.1007/s10008-014-2420-4) contains supplementary material, which is available to authorized users.

J. L. Ropero-Vega (✉) · M. E. Niño-Gómez
Centro de Investigaciones en Catálisis—CICAT, Centro de Materiales y Nanociencias - CMN, Universidad Industrial de Santander, Sede Guatiguará, Calle 8N No. 3W-60 El Refugio, C.P. 681011 Piedecuesta, Santander, Colombia
e-mail: jlropero@ciencias.uis.edu.co

M. E. Niño-Gómez
e-mail: marthan@uis.edu.co

A. M. Meléndez · J. A. Pedraza-Avella
Grupo de Investigaciones en Minerales, Biohidrometalurgia y Ambiente—GIMBA, Centro de Materiales y Nanociencias—CMN, Universidad Industrial de Santander, Sede Guatiguará, Calle 8N No. 3W-60 El Refugio, C.P. 681011 Piedecuesta, Santander, Colombia

R. J. Candal
Instituto de Química Física de Materiales, Medio Ambiente y Energía—INQUIMAE, Universidad de Buenos Aires, Ciudad Universitaria Pabellón 2, C1428EHA Buenos Aires, Argentina

## Introduction

Since Fujishima and Honda [1] reported the photoinduced water splitting on a $TiO_2$ electrode under irradiation in 1972, photoelectrolysis has attracted much attention and has been widely studied with the aim of applying this process in solar energy conversion [2–7]. All this is focused on dealing with the problems of environmental remediation and production of clean and renewable fuels (e.g., hydrogen) [5, 8].

In recent years, research efforts have focused on development of new semiconductor materials capable of being excited by visible light radiation [9]. Researchers have explored different strategies in the design of catalysts as in the case of coupled semiconductors as $WO_3$-$TiO_2$- [10, 11] and $Bi_2O_3$-$TiO_2$-doped [12–14] semiconductors, among them highlight mainly non-metal and transition-metal-doped $TiO_2$ (N, S, Fe, or Cr) [15, 16], and mixed metal oxide semiconductors (binary, ternary, or quaternary) [17]. Among the latter, bismuth-

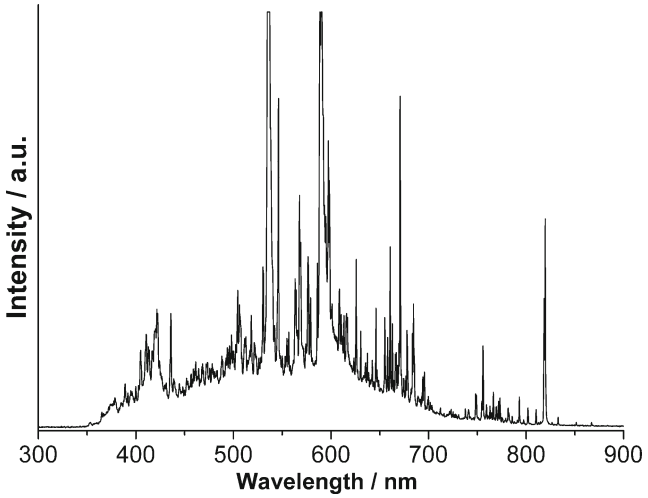


**Fig. 1** Emission spectrum of the visible light source

**Table 1** Elemental analysis by SEM-EDS of the Bi-Nb-M-O/304 SS (M = Al, Fe, Ga, In) films. All values are reported in atomic percentages

| Film | Inside the agglomerates | | | Outside the agglomerates | | |
|---|---|---|---|---|---|---|
| | Bi | Nb | M | Bi | Nb | M |
| Bi-Nb-Al-O/304 SS | 26.5 | 0.4 | 2.1 | 0.5 | N.A. | 0.7 |
| Bi-Nb-Fe-O/304 SS | 16.3 | 1.6 | 22.8[a] | 1.0 | 0.6 | 61.7[a] |
| Bi-Nb-Ga-O/304 SS | 25.8 | 0.3 | 2.6 | 0.4 | N.A. | 1.0 |
| Bi-Nb-In-O/304 SS | 29.8 | 1.6 | 0.9 | 1.0 | 0.5 | 1.2 |

[a] The percentage value of Fe includes the contribution made by the stainless steel support

*N.A.* data not available

based mixed oxide semiconductors have attracted interest due to their excellent stability, visible light absorption, and photocatalytic properties [18–26]. These include, among others, bismuth oxide ($Bi_2O_3$) [18], bismuth niobate ($Bi_3NbO_7$) [26], perovskite-type bismuth ferrite ($BiFeO_3$) [19], and sillenite-type $Bi_{25}GaO_{39}$ [27] and $Bi_{25}FeO_{40}$ [28].

Mixed oxides of $Bi_2MNbO_7$ (M = Al, Fe, Ga, In) with pyrochlore crystalline structure are a type of semiconductor materials of the Bi-Nb-M-O system [29–31]. These semiconductor oxides are very promising as photocatalyst due to their structural, optical, and electrical transport properties [31–34]. They were prepared as powders initially by solid-state reaction [29–32] and then by the sol–gel method [35] and metal-organic decomposition processes [36]. In our research groups, we have prepared a series of mixed oxide semiconductor films of the Bi-Nb-M-O system (M = Al, Fe, Ga, In) which have presented good physical, optical, photocatalytic, and photoelectrocatalytic properties [37–40]. However, the films in fact consist of a mixture of mixed oxides, which had not been identified so far, so it is not possible to define a correct structure for this material. For this reason, we refer to these materials as mixed oxide semiconductor films of Bi-Nb-M-O (M = Al, Fe, Ga, In). Despite all the above, the films exhibit visible light absorption properties and presented good photocatalytic activity in the oxidation of methyl orange [37, 38]. Additionally, these mixed oxide films were used as photoanodes in the photoelectrochemical hydrogen production from alkaline solutions containing cyanide showing a marked increase in their activities compared with the analogous electrochemical process (in the dark) [39, 40]. Nevertheless, the obtained results cannot be straightforward correlated with the optical or structural properties of the films, and apparently the photoelectrochemical properties have a major contribution in this behavior.

Therefore, in this work, we report the structural characterization and photoelectrochemical properties of Bi-Nb-M-O (M = Al, Fe, Ga, In) films prepared on stainless steel in order to explore their potential application as photoelectrochemical materials. The structural properties of the films were studied by SEM-EDS, XRD, and XPS. The electrochemical behavior was evaluated by cyclic voltammetry, and the photoresponse and stability of the films were studied by open circuit potential and linear sweep voltammetry measurements.

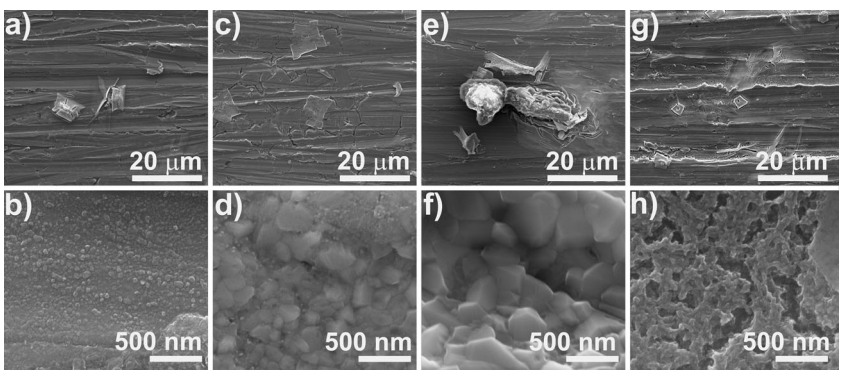


**Fig. 2** SEM micrographs of the films: **a**, **b** Bi-Nb-Al-O/304 SS, **c**, **d** Bi-Nb-Fe-O/304 SS, **e**, **f** Bi-Nb-Ga-O/304 SS, **g**, **h** Bi-Nb-In-O/304 SS

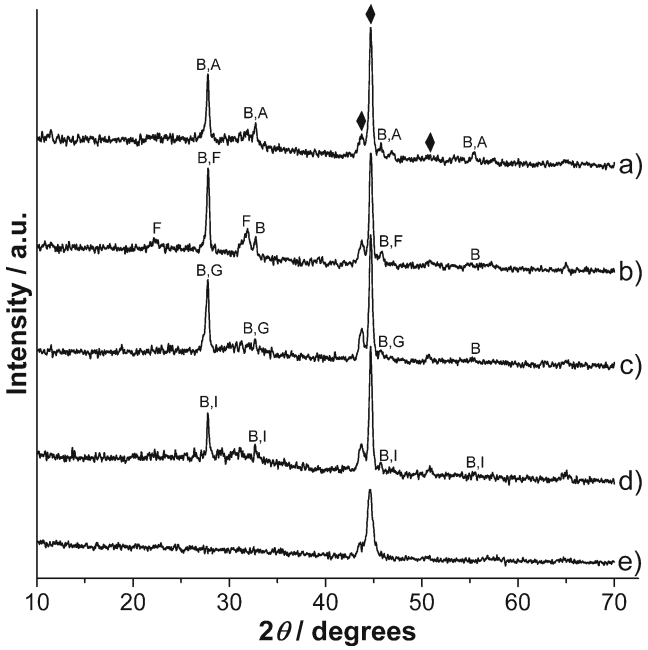


**Fig. 3** XRD profiles of **a** Bi-Nb-Al-O/304 SS, **b** Bi-Nb-Fe-O/304 SS, **c** Bi-Nb-Ga-O/304 SS, **d** Bi-Nb-In-O/304 SS, and **e** 304 SS plate annealed at 500 °C (used as reference)

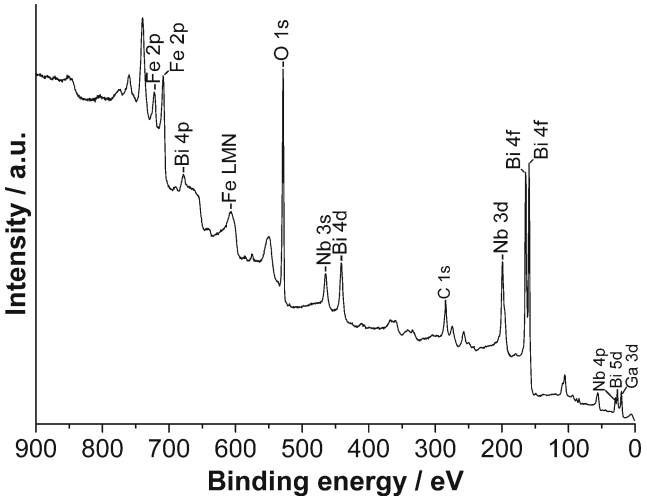


**Fig. 4** XPS spectrum of Bi-Nb-Ga-O/304 SS film

## Experimental

Mixed oxide semiconductor films of Bi-Nb-M-O (M = Al, Fe, Ga, In) were prepared by dip-coating on AISI/SAE 304 stainless steel (304 SS) plates (2.0 cm×2.0 cm). Details of the sol preparation were published previously [37]. The films were obtained at a withdrawal speed of 10.0 cm/min, dried at room temperature (25 °C) for 1 h, and finally annealed in air at 500 °C for 4 h.

Scanning electron microscopy (SEM) micrographs of the films (Bi-Nb-M-O/304 SS) were obtained with a Quanta Field Emission Gun microscope (model 650) equipped with an EDAX Apollo X energy-dispersive X-ray spectroscopy (EDS) detector operated at 5, 8, and 10 kV in second electron mode. X-ray diffraction (XRD) profiles were collected on a Bruker D8 Discover diffractometer operated at 40 kV and 30 mA, using Cu Kα radiation (1.540598 Å) selected with Ni filter, in grazing incidence mode with a step of 0.015° and a counting time of 1.0 s per step. X-ray photoelectron spectroscopy (XPS) analysis was performed in a Physical Electronics 1257 system using monochromatic Al Kα radiation (1,486.6 eV). Bismuth, niobium, aluminum, iron, gallium, indium, and oxygen peaks were deconvoluted into several components by fitting the experimental data to Gaussian-Lorentzian curves. The XPS peaks were referred to the position of the C1s peak at 284.5 eV. In all XPS measurements, the photoelectrons were collected perpendicularly to the surface sample.

Electrochemical measurements of the films were performed with a Gamry Reference 600 Potentiostat/Galvanostat/ZRA (Gamry Instruments) using a conventional three-electrode cell. A saturated calomel electrode and a graphite bar were used as reference and counter electrode, respectively. However, all the potentials reported are referred to the normal hydrogen electrode (NHE). The geometric area of the working electrode (Bi-Nb-M-O/304 SS film) was 3.0 $cm^2$. The electrochemical behavior of the films was studied by cyclic voltammetry (CV) measurements in 60 mL of an aqueous solution of $Na_2SO_4$ (0.1 M) at pH 8.5. The photoresponse of the films was evaluated by open circuit potential (OCP) and linear sweep voltammetry (LSV) measurements with chopped visible light irradiation. The electrolytic solution (60 mL) was an aqueous solution of $NaClO_4$ (0.1 M) at pH 8.5. In all cases, the system was purged with nitrogen and stirred for 20 min before each test. A metal halide lamp (Philips MHN-TD, 150 W) was used as visible light radiation source. The emission spectrum of the lamp is shown in Fig. 1. All the electrochemical experiments were performed at room temperature (25 °C).

**Table 2** The crystalline phases found in Bi-Nb-M-O/304 SS (M = Al, Fe, Ga, In) films

| Film | Crystalline phase found | PDF number |
|---|---|---|
| Bi-Nb-Al-O/304 SS | $Bi_2O_3$ (B) | 76-0147 |
| | $Bi_{24}Al_2O_{39}$ (A) | 42-0184 |
| Bi-Nb-Fe-O/304 SS | $Bi_2O_3$ (B) | 76-0147 |
| | $BiFeO_3$ (F) | 71-2494 |
| Bi-Nb-Ga-O/304 SS | $Bi_2O_3$ (B) | 76-0147 |
| | $Bi_{25}GaO_{39}$ (G) | 79-0767 |
| Bi-Nb-In-O/304 SS | $Bi_2O_3$ (B) | 76-0147 |
| | $Bi_{35}InO_{54}$ (I) | 42-0188 |

**Table 3** Binding energies (eV) of Bi-Nb-M-O/304 SS films

| Film | Bi ($4f_{7/2}$) | Bi ($4f_{5/2}$) | Nb ($3d_{3/2}$) | Nb ($3d_{5/2}$) | O (1 s) | M |
|---|---|---|---|---|---|---|
| Bi-Nb-Al-O/304 SS | 159.0 | 164.3 | 206.8 | 209.6 | 529.5<br>531.5 | 73.8 (Al 2p) |
| Bi-Nb-Fe-O/304 SS | 158.3 | 163.6 | 206.1 | 208.8 | 529.8<br>531.8 | 710.3 (Fe $2p_{3/2}$) |
| Bi-Nb-Ga-O/304 SS | 159.2 | 164.4 | 207.0 | 209.8 | 529.4<br>531.3 | 20.0 (Ga 3d)<br>1,118.1 (Ga $2p_{3/2}$) |
| Bi-Nb-In-O/304 SS | 159.0 | 164.3 | 206.9 | 209.6 | 529.7<br>531.5 | 444.8 (In $3d_{5/2}$)<br>452.3 (In $3d_{3/2}$) |

## Results and discussion

### Scanning electron microscopy

The morphology of mixed oxide films of Bi-Nb-M-O/304 SS (M = Al, Fe, Ga, In) was analyzed by SEM, and the results are shown in Fig. 2.

The micrographs on top show that the surface of the films is rough and with agglomerates distributed in all the analyzed area. EDS analyses reveal that the films are composed of Bi, Nb, and M (Al, Fe, Ga, or In), while the agglomerates are mainly composed of Bi with a minor amount of Nb and M (see Table 1). Furthermore, these agglomerates are composed of particles with irregular size and shape, as shown in Fig. 2

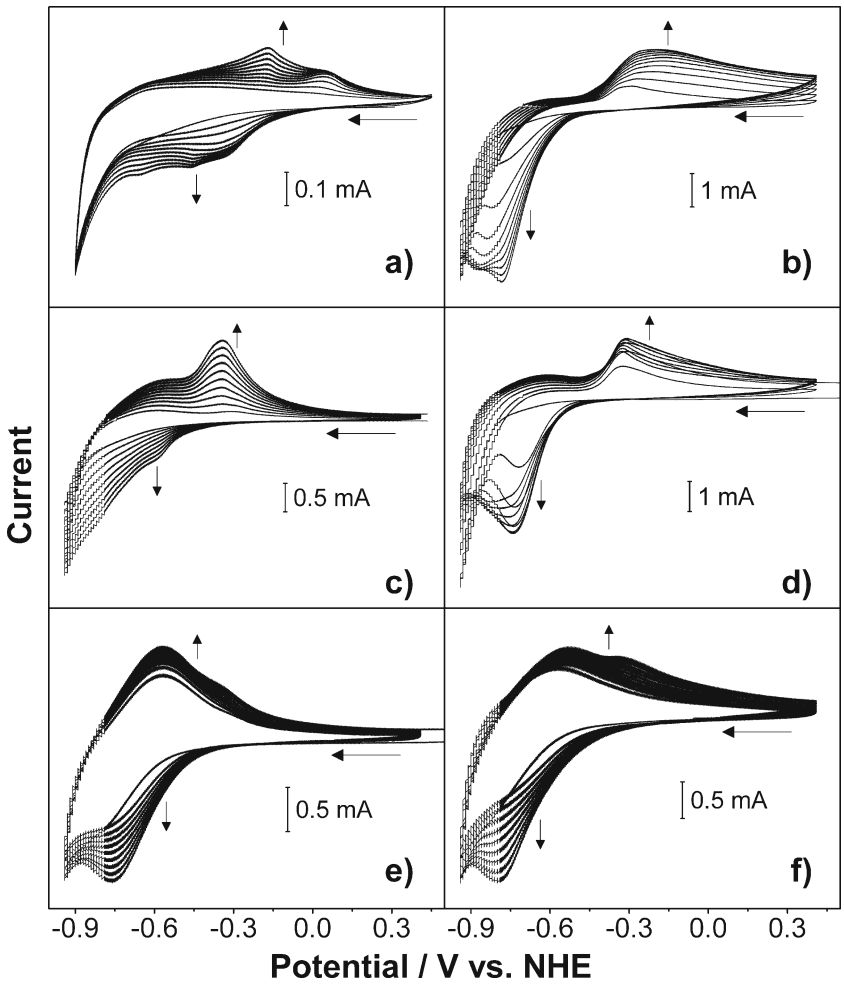


**Fig. 5** Cyclic voltammograms of **a** 304 SS plate, **b** $Bi_2O_3$/304 SS, **c** Bi-Nb-Al-O/304 SS, **d** Bi-Nb-Fe-O/304 SS, **e** Bi-Nb-Ga-O/304 SS, and **f** Bi-Nb-In-O/304 SS films (0.1 M of $Na_2SO_4$; pH 8.5, 100 mV/s)

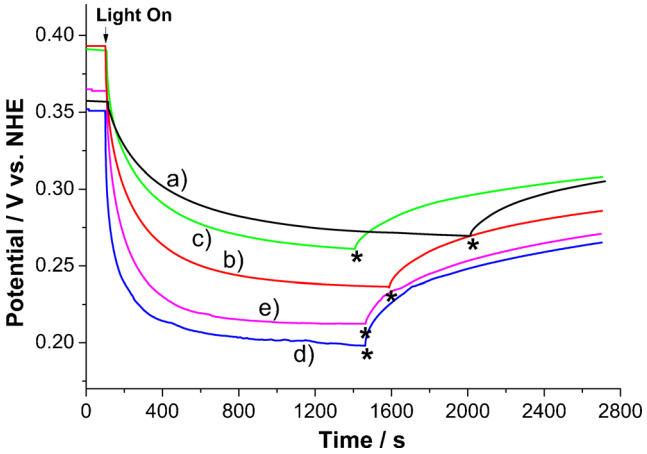


**Fig. 6** Open circuit potential measurement versus time under visible light irradiation: **a** $Bi_2O_3$/304 SS, **b** Bi-Nb-Al-O/304 SS, **c** Bi-Nb-Fe-O/304 SS, **d** Bi-Nb-Ga-O/304 SS, and **e** Bi-Nb-In-O/304 SS (0.1 M of $NaClO_4$; pH 8.5)

(bottom). EDS spectra were included as supplementary material. It is worth highlighting that the results provided by EDS analyses are qualitative and depend on the distribution of elements in the surface, its uniformity and homogeneity, so it cannot be taken as overall performance if only one portion of the surface is being observed.

## X-ray diffraction

XRD profiles of mixed oxide films of Bi-Nb-M-O/304 SS (M = Al, Fe, Ga, In) are shown in Fig. 3. The reflections present at 43.7, 44.7, and 50.7° correspond to the 304 SS support (marked with black diamond) [41]. The other reflections shown in the profiles were analyzed by comparing the observed profile with the patterns reported in the PDF-2 database of the International Center for Diffraction Data (ICDD). The crystalline phases found in each of the films are shown in Table 2.

The presence of $Bi_2O_3$ was observed in all the films. The aforementioned oxides have been investigated for photocatalytic applications due to its visible light adsorption properties. Bismuth oxide ($Bi_2O_3$, $E_g$~2.8 eV) has been studied in the oxidation of model pollutant (methyl orange [18, 42] and rhodamine B [43, 44]) as well as the production of renewable energies such as hydrogen [45]. Sillenite-type $Bi_{25}GaO_{39}$ ($E_g$~2.95 eV) has exhibited comparable photocatalytic behavior on the oxidation of methylene blue than $TiO_2$ [27], whereas perovskite-type $BiFeO_3$ is a bismuth-iron-based compound with good photocatalytic properties under visible light due to their low band-gap (2.18) [19]. The photophysical or photocatalytic properties of $Bi_{24}Al_2O_{39}$ and $Bi_{35}InO_{54}$, to our knowledge, have not been studied so far.

## X-ray photoelectron spectroscopy

XPS measurements of mixed oxide films of Bi-Nb-M-O/304 SS (M = Al, Fe, Ga, In) were performed to investigate the surface chemistry. The XPS spectrum of Bi-Nb-Ga-O/304 SS film is shown in Fig. 4. The XPS spectra corresponding to Bi 4f, Nb 3d, O 1s, and M (Al 2p, Fe 2p, Ga 2p, Ga 3d, and In 3d) for each of the film were included as supplementary material.

It can be seen in Fig. 4 that the surface of the film is mainly composed by Bi, Ga, and Nb elements. The presence of Fe element is due to 304 SS support. The composition of the other films was similar. The binding energy (BE) values for all the films are given in Table 3.

The BE values for Bi $4f_{7/2}$ and Bi $4f_{5/2}$ demonstrated that Bi species are present in the form of Bi(III) [12, 13]. The BE values for Nb ($3d_{3/2}$ and $3d_{5/2}$) [46], Al (2p) [47], Fe ($2p_{3/2}$) [48], Ga (3d and $2p_{3/2}$) [49], and In ($3d_{5/2}$ and $3d_{3/2}$) [50] correspond to Nb(V), Al(III), Fe(III), Ga(III), and In(III), respectively, as reported in the literature. In the case of oxygen

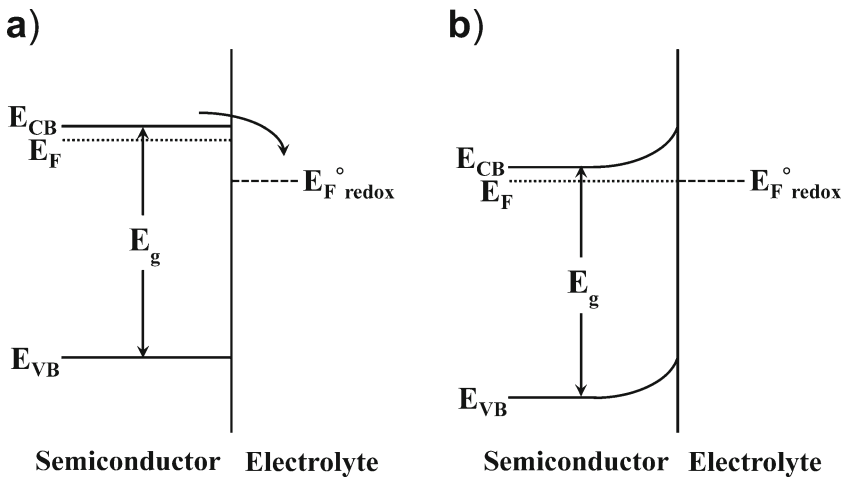


**Fig. 7** Energy diagram of an n-type semiconductor **a** before and **b** after of contact with an aqueous electrolyte

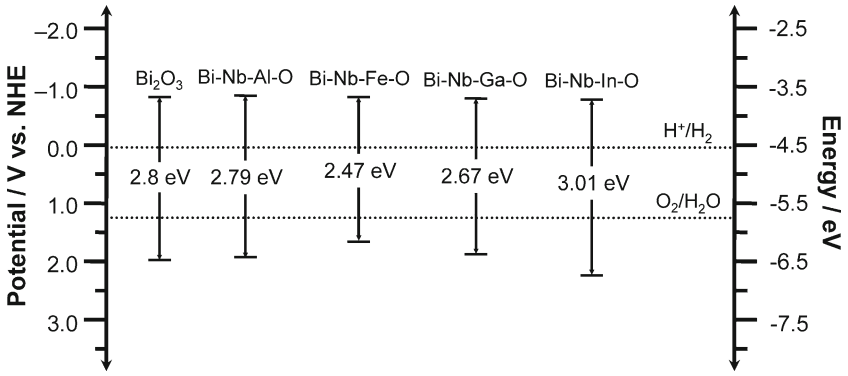


**Fig. 8** Schematic illustration of calculated energy positions of valence and conduction band edges at pH 0 of the films prepared

atom, the lower BE (529.6±0.2) is attributed to metal-O bonding (metal = Bi, Nb, Al, Fe, Ga, In), and the higher BE (531.5±0.3) is related to O-H surface group.

## Electrochemical properties

Cyclic voltammetry was used in order to explore the electrochemical behavior of the films at pH 8.5. Cyclic voltammograms of the Bi-Nb-M-O/304 SS films recorded under dark are shown in Fig. 5. The voltammograms of a 304 SS plate annealed at 500 °C and $Bi_2O_3$/304 SS film was also included for comparative purposes. This film was prepared using the same procedure as described for Bi-Nb-M-O/304 SS films but without using the Nb and M precursors.

The voltammogram of 304 SS plate (Fig. 5a) shows the presence of oxidation-reduction processes related principally to Fe species. It can be seen that the voltammograms of all the films are different and not have the same anodic-cathodic peaks, indicating that there was a good coating of the support. The only anodic peak observed in the voltammograms of the films is related to oxidation of Bi(III) [51]. The shape of the voltammograms of Bi-Nb-Al-O/304 SS and Bi-Nb-Fe-O/304 SS films (Fig. 5c, d) is similar to the $Bi_2O_3$/304 SS film (Fig. 5b). However, the anodic peak grows more rapidly with each scan cycle in the Bi-Nb-Al-O/304 SS film, which indicates that this material has greater corrosion. On the other hand, the position and shape of the anodic peak change for the Bi-Nb-Ga-O/304 SS and Bi-Nb-In-O/304 SS films (Fig. 5e, f).

Open circuit potential (OCP) measurements of the films as a function of time under visible light irradiation are shown in Fig. 6. The results for a $Bi_2O_3$/304 SS film are shown by comparative purposes.

It can be observed that in all cases, the lighting of the films changes the OCP toward less positive values. When an n-type semiconductor immersed in an aqueous electrolyte is

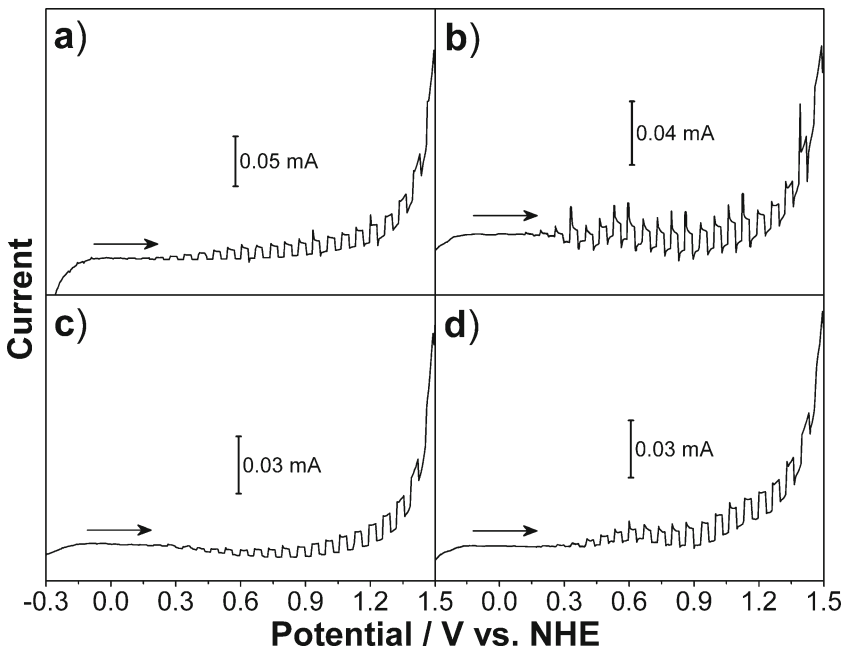


**Fig. 9** Linear sweep voltammograms with chopped visible light irradiation of **a** Bi-Nb-Al-O/304 SS, **b** Bi-Nb-Fe-O/304 SS, **c** Bi-Nb-Ga-O/304 SS, and **d** Bi-Nb-In-O/304 SS films (0.1 M of $NaClO_4$; pH 8.5; 50 mV/s)

illuminated with radiation of equal or higher energy to its band-gap, electron–hole pairs ($e^-$-$h^+$) are generated. These photogenerated charge carriers can promote oxidation-reduction reactions at the semiconductor/electrolyte solution interface [52, 53]. The electrons are accumulated in the conduction band of the semiconductor, which generates a decrease of the OCP values. The photogenerated holes can travel to the semiconductor/electrolyte interface where they can react with absorbed hydroxyl groups ($OH^-$) producing hydroxyl radicals ($^{\bullet}OH$). These radicals can oxidize adsorbed species on the semiconductor surface (indirect photocatalysis). On the other hand, the adsorbed species can be oxidized directly by holes (direct photocatalysis). Meanwhile, the electrons in the conduction band can reduce oxygen ($O_2$) to form superoxide anion radicals ($^{\bullet}O_2^-$) [54]. Therefore, the mixed oxide films of Bi-Nb-M-O/304 SS (M = Al, Fe, Ga, In) exhibited a typical n-type semiconductor behavior.

It is well known that for an n-type semiconductor, the position of the Fermi level ($E_F$) is located just below the potential of conduction band ($E_{CB}$) (Fig. 7a). When the semiconductor comes into contact with an aqueous solution in the absence of an external potential (i.e., OCP), the Fermi levels of the semiconductor and the electrolyte (redox potential, $E_{F\,redox}$) are equal (Fig. 7b) [55, 56].

Taking into account the above, it is possible to schematize the potentials of valence and conduction bands for the Bi-Nb-M-O/304 SS films, as shown in Fig. 8. The band-gap values of the films were determined experimentally and published elsewhere [37] (see supplementary material for details).

It can be observed in Fig. 8 that the $E_{CB}$ values are similar for all the Bi-Nb-M-O/304 SS films and in turn are near to the $E_{CB}$ value of $Bi_2O_3$. Therefore, the photoelectrochemical properties of the films indicate that they have bismuth oxide nature. Nevertheless, the addition of metal oxides in the bismuth oxide structure (i.e., Al, Fe, Ga, and In-based oxides) changes the $E_{VB}$ value of the material, modifying its oxidative capacity. According to the above, the ability of the films to carry out photolysis of water would be given by the following performance: Bi-Nb-Fe-O/304 SS>Bi-Nb-Ga-O/304 SS≈Bi-Nb-Al-O/304 SS>Bi-Nb-In-O/304 SS.

The photoresponse of the Bi-Nb-M-O/304 SS (M = Al, Fe, Ga, In) films was evaluated by linear sweep voltammetry with chopped visible light irradiation, and the results are shown in Fig. 9. These photovoltammetry experiments can be used to evaluate both of the electrochemical (in dark) and the photoelectrochemical (under light irradiation) behavior of the films under the same experimental conditions [57].

All the voltammograms show an increase in the photocurrent in the anodic direction which is indicative of n-type semiconductors. This is consistent with the results obtained in the OCP measurements. It can be seen that the rise and fall of the photocurrent correspond to the irradiation being switched on and off, respectively. It should be noted that after illumination, there is a photocurrent increase and then declines to a steady-state value. The onset of the photocurrent is close to +0.1 V for all the films. Below this value, the rate of electron–hole recombination is high, which does not generate a photocurrent [58]. There was not observed current in dark since the onset of the photocurrent until much more positive potentials. Furthermore, the photocurrent is dependent of the potential and increases as the applied potential increases. All the above indicates that these materials may be promising for use in photoelectrochemical cells.

## Conclusions

The surface of the films is rough and composed of agglomerates distributed in all the analyzed area. The SEM-EDS analyses reveal that the surface of the films is composed by Bi with a minor amount of Nb and M (Al, Fe, Ga, or In). All the films are composed principally of a mixture of $Bi_2O_3$ and a Bi-M-based mixed oxide which most of them have visible light absorption properties. The presence of any Nb-containing oxide crystalline phase was not evidenced; probably the niobium is doping the bismuth oxides.

The response in the anodic region was good for all the films which indicate that these materials can be used in photoelectrochemical processes.

**Acknowledgments** This work has been carried out with the financial support of Universidad Industrial de Santander (DIEF Ciencias, Project 5185). J.L. Ropero-Vega thanks COLCIENCIAS for the doctoral scholarship in the frame of the program "Convocatoria nacional para estudios a nivel de doctorado en Colombia—año 2009". The authors thank Jonathan I. Avila for the XPS analyses.

## References

1. Fujishima A, Honda K (1972) Electrochemical photolysis of water at a semiconductor electrode. Nature 238:37–38
2. Aruchamy A, Aravamudan G, Subba Rao GV (1982) Semiconductor based photoelectrochemical cells for solar energy conversion—an overview. Bull Mater Sci 4:483–526
3. Tryk DA, Fujishima A, Honda K (2000) Recent topics in photoelectrochemistry: achievements and future prospects. Electrochim Acta 45:2363–2376
4. Grätzel M (2001) Photoelectrochemical cells. Nature 414:338–344
5. Zhang H, Chen G, Bahnemann DW (2009) Photoelectrocatalytic materials for environmental applications. J Mater Chem 19:5089–5121
6. Lianos P (2011) Production of electricity and hydrogen by photocatalytic degradation of organic wastes in a photoelectrochemical cell. J Hazard Mater 185:575–590
7. Ochiai T, Fujishima A (2012) Photoelectrochemical properties of $TiO_2$ photocatalyst and its applications for environmental purification. J Photochem Photobiol C 13:247–262

8. Li Y, Zhang JZ (2009) Hydrogen generation from photoelectrochemical water splitting based on nanomaterials. Laser Photonics Rev 4:517–528
9. Navarro RM, del Valle F, Villoria de la Mano JA, Álvarez-Galván M, Fierro J (2009) Photocatalytic water splitting under visible light. Advances in chemical engineering. Elsevier, pp. 111–143
10. Georgieva J, Valova E, Armyanov S, Philippidis N, Poulios I, Sotiropoulos S (2012) Bi-component semiconductor oxide photoanodes for the photoelectrocatalytic oxidation of organic solutes and vapours: a short review with emphasis to $TiO_2$–$WO_3$ photoanodes. J Hazard Mater 211–212:30–46
11. Riboni F, Bettini LG, Bahnemann DW, Selli E (2013) $WO_3$-$TiO_2$ vs. $TiO_2$ photocatalysts: effect of the W precursor and amount on the photocatalytic activity of mixed oxides. Catal Today 209:28–34
12. Bian Z, Zhu J, Wang S, Cao Y, Qian X, Li H (2008) Self-assembly of active $Bi_2O_3$/$TiO_2$ visible photocatalyst with ordered mesoporous structure and highly crystallized anatase. J Phys Chem C 112:6258–6262
13. Xu J, Ao Y, Fu D, Yuan C (2008) Synthesis of $Bi_2O_3$-$TiO_2$ composite film with high-photocatalytic activity under sunlight irradiation. Appl Surf Sci 255:2365–2369
14. Zhao X, Liu H, Qu J (2011) Photoelectrocatalytic degradation of organic contaminants at $Bi_2O_3$/$TiO_2$ nanotube array electrode. Appl Surf Sci 257:4621–4624
15. Ohno T, Miyamoto Z, Nishijima K, Kanemitsu H, Xueyuan F (2006) Sensitization of photocatalytic activity of S- or N-doped $TiO_2$ particles by adsorbing $Fe^{3+}$ cations. Appl Catal A 302:62–68
16. Dholam R, Patel N, Adami M, Miotello A (2009) Hydrogen production by photocatalytic water-splitting using Cr- or Fe-doped $TiO_2$ composite thin films photocatalyst. Int J Hydrog Energy 34:5337–5346
17. Di Paola A, García-López E, Marcì G, Palmisano L (2012) A survey of photocatalytic materials for environmental remediation. J Hazard Mater 211–212:3–29
18. Zhang L, Wang W, Yang J, Chen Z, Zhang W, Zhou L, Liu S (2006) Sonochemical synthesis of nanocrystallite $Bi_2O_3$ as a visible-light-driven photocatalyst. Appl Catal, A 308:105–110
19. Gao F, Chen XY, Yin KB, Dong S, Ren Z, Yuan F, Yu T, Zou Z, Liu J (2007) Visible-light photocatalytic properties of weak magnetic $BiFeO_3$ nanoparticles. Adv Mater 19:2889–2892
20. Wang W, Li N, Chi Y, Li Y, Yan W, Li X, Shao C (2013) Electrospinning of magnetical bismuth ferrite nanofibers with photocatalytic activity. Ceram Int 39:3511–3518
21. Soltani T, Entezari MH (2013) Sono-synthesis of bismuth ferrite nanoparticles with high photocatalytic activity in degradation of rhodamine B under solar light irradiation. Chem Eng J 223:145–154
22. Wang X, Lin Y, Ding X, Jiang J (2011) Enhanced visible-light-response photocatalytic activity of bismuth ferrite nanoparticles. J Alloys Compd 509:6585–6588
23. Fang J, Ma J, Sun Y, Liu Z, Gao C (2011) Synthesis of $Bi_3NbO_7$ nanoparticles with a hollow structure and their photocatalytic activity under visible light. Solid State Sci 13:1649–1653
24. Zhang G, Yang J, Zhang S, Xiong Q, Huang B, Wang J, Gong W (2009) Preparation of nanosized $Bi_3NbO_7$ and its visible-light photocatalytic property. J Hazard Mater 172:986–992
25. Ai Z, Ho W, Lee S (2012) A stable single-crystal $Bi_3NbO_7$ nanoplates superstructure for effective visible-light-driven photocatalytic removal of nitric oxide. Appl Surf Sci 263:266–272
26. Wang L, Wang W, Shang M, Sun S, Yin W, Ren J, Zhou J (2010) Visible light responsive bismuth niobate photocatalyst: enhanced contaminant degradation and hydrogen generation. J Mater Chem 20:8405–8410
27. Lin X, Huang F, Wang W, Xia Y, Wang Y, Liu M, Shi J (2008) Photocatalytic activity of a sillenite-type material $Bi_{25}GaO_{39}$. Catal Commun 9:572–576
28. Zhang CY, Sun HJ, Chen W, Zhou J, Li B, Wang Y (2009) Hydrothermal synthesis and photo-catalytic property of $Bi_{25}FeO_{40}$ powders. Applications of Ferroelectrics. IEEE, pp 1–3
29. Zou Z, Ye J, Arakawa H (2000) Synthesis, magnetic and electrical transport properties of the $Bi_2InNbO_7$ compound. Solid State Commun 116:259–263
30. Zou Z, Ye J, Arakawa H (2001) Preparation, structural and optical properties of a new class of compounds, $Bi_2MNbO_7$ (M = Al, Ga, In). Mater Sci Eng B 79:83–85
31. Zou Z, Ye J, Arakawa H (2001) Substitution effects of $In^{3+}$ by $Fe^{3+}$ on photocatalytic and structural properties of $Bi_2InNbO_7$ photocatalysts. J Mol Catal A Chem 168:289–297
32. Zou Z, Ye J, Arakawa H (2003) Photocatalytic water splitting into $H_2$ and/or $O_2$ under UV and visible light irradiation with a semiconductor photocatalyst. Int J Hydrog Energy 28:663–669
33. Zou Z, Ye J, Arakawa H (2001) Photocatalytic and photophysical properties of a novel series of solid photocatalysts, $Bi_2MNbO_7$ ($M=Al^{3+}$, $Ga^{3+}$ and $In^{3+}$). Chem Phys Lett 333:57–62
34. Zou Z, Ye J, Arakawa H (2001) Substitution effects of $In^{3+}$ by $Al^{3+}$ and $Ga^{3+}$ on the photocatalytic and structural properties of the $Bi_2InNbO_7$ photocatalyst. Chem Mater 13:1765–1769
35. Garza-Tovar LL, Torres-Martínez LM, Rodríguez DB, Gómez R, del Angel G (2006) Photocatalytic degradation of methylene blue on $Bi_2MNbO_7$ (M = Al, Fe, In, Sm) sol–gel catalysts. J Mol Catal A Chem 247:283–290
36. Teixeira Z, Otubo L, Gouveia RF, Alves OL (2010) Preparation and characterization of powders and thin films of $Bi_2AlNbO_7$ and $Bi_2InNbO_7$ pyrochlore oxides. Mater Chem Phys 124:552–557
37. Ropero-Vega JL, Rosas-Barrera KL, Pedraza-Avella JA, Laverde-Cataño DA, Pedraza-Rosas JE, Niño-Gómez ME (2010) Photophysical and photocatalytic properties of $Bi_2MNbO_7$ (M=Al, In, Ga, Fe) thin films prepared by dip-coating. Mater Sci Eng B 174:196–199
38. Rosas-Barrera KL, Ropero-Vega JL, Pedraza-Avella JA, Niño-Gómez ME, Pedraza-Rosas JE, Laverde-Cataño DA (2011) Photocatalytic degradation of methyl orange using $Bi_2MNbO_7$ (M=Al, Fe, Ga, In) semiconductor films on stainless steel. Catal Today 166:135–139
39. Pedraza-Avella JA, Rosas-Barrera KL, Pedraza-Rosas JE, Laverde-Cataño DA (2011) Photoelectrochemical hydrogen production from aqueous solution containing cyanide using $Bi_2MNbO_7$ (M=Al, Fe, Ga, In) films on stainless steel as photoanodes. Top Catal 54:244–249
40. Rosas-Barrera KL, Pedraza-Avella JA, Ballén-Gaitán BP, Cortés-Peña J, Pedraza-Rosas JE, Laverde-Cataño DA (2011) Photoelectrolytic hydrogen production using $Bi_2MNbO_7$ (M=Al, Ga) semiconductor film electrodes prepared by dip-coating. Mater Sci Eng B 176:1359–1363
41. Sokolov S, Ortel E, Radnik J, Kraehnert R (2009) Influence of steel composition and pre-treatment conditions on morphology and microstructure of $TiO_2$ mesoporous layers produced by dip coating on steel substrates. Thin Solid Films 518:27–35
42. Iyyapushpam S, Nishanthi ST, Pathinettam Padiyan D (2013) Photocatalytic degradation of methyl orange using $\alpha$-$Bi_2O_3$ prepared without surfactant. J Alloys Compd 563:104–107
43. Weidong H, Wei Q, Xiaohong W, Xianbo D, Long C, Zhaohua J (2007) The photocatalytic properties of bismuth oxide films prepared through the sol–gel method. Thin Solid Films 515:5362–5365
44. Brezesinski K, Ostermann R, Hartmann P, Perlich J, Brezesinski T (2010) Exceptional photocatalytic activity of ordered mesoporous $\beta$-$Bi_2O_3$ thin films and electrospun nanofiber mats. Chem Mater 22:3079–3085
45. Gurunathan K (2004) Photocatalytic hydrogen production using transition metal ions-doped $\gamma$-$Bi_2O_3$ semiconductor particles. Int J Hydrog Energy 29:933–940

46. Xia J, Masaki N, Jiang K, Yanagida S (2007) Sputtered $Nb_2O_5$ as a novel blocking layer at conducting glass/$TiO_2$ interfaces in dye-sensitized ionic liquid solar cells. J Phys Chem C 111:8092–8097
47. Innocenzi P, Martucci A, Armelao L, Licoccia S, Di Vona M, Traversa E (2000) Sol–gel synthesis of β-$Al_2TiO_5$ thin films at low temperature. Chem Mater 12:517–524
48. Fujii T, De Groot FMF, Sawatzky GA, Voogt F, Hibma T, Okada K (1999) In situ XPS analysis of various iron oxide films grown by $NO_2$-assisted molecular-beam epitaxy. Phys Rev B 59:3195–3202
49. Valet M, Hoffman DM (2001) Synthesis of homoleptic gallium alkoxide complexes and the chemical vapor deposition of gallium oxide films. Chem Mater 13:2135–2143
50. Poznyak SK, Kulak AI (2000) Characterization and photoelectrochemical properties of nanocrystalline $In_2O_3$ film electrodes. Electrochim Acta 45:1595–1605
51. Vivier V, Régis A, Sagon G, Nedelec J, Yu L, Cachet-Vivier C (2001) Cyclic voltammetry study of bismuth oxide $Bi_2O_3$ powder by means of a cavity microelectrode coupled with Raman microspectrometry. Electrochim Acta 46:907–914
52. Aroutiounian VM, Arakelyan VM, Shahnazaryan GE (2005) Metal oxide photoelectrodes for hydrogen generation using solar radiation-driven water splitting. Sol Energy 78:581–592
53. Lei C-X, Zhou H, Wang C, Feng Z-D (2013) Self-assembly of ordered mesoporous $TiO_2$ thin films as photoanodes for cathodic protection of stainless steel. Electrochim Acta 87:245–249
54. Straka L, Yagodzinskyy Y, Kawakami H, Romu J, Ilola R, Hänninen H (2008) Open-circuit potential as an indicator of damage of atomic layer deposited $TiO_2$ on AISI 304 stainless steel. Thin Solid Films 517:641–647
55. Memming R (1988) Photoelectrochemical solar energy conversion. In: Steckhan E (ed) Electrochemistry II. Springer, Berlin, pp 79–112
56. Xu Y, Schoonen MA (2000) The absolute energy positions of conduction and valence bands of selected semiconducting minerals. Am Mineral 85:543–556
57. De Tacconi NR, Chenthamarakshan CR, Yogeeswaran G, Watcharenwong A, de Zoysa R, Basit N, Rajeshwar K (2006) Nanoporous TiO2 and WO3 films by anodization of titanium and tungsten substrates: influence of process variables on morphology and photoelectrochemical response. J Phys Chem B 110:25347–25355
58. McShane CM, Choi K-S (2009) Photocurrent enhancement of n-type $Cu_2O$ electrodes achieved by controlling dendritic branching growth. J Am Chem Soc 131:2561–2569